

ESVM : An Open-source Electrostatic Vlasov-Maxwell Code

Michaël J TOUATI^{1, 2, 3}

¹ Department of Electrical Engineering, University of California Los Angeles, Los Angeles, CA 90095, USA ² Group of Lasers and Plasmas, IPFN, IST, Universidade de Lisboa, Lisbon, Portugal ³ Centro de Láseres Pulsados de Salamanca (CLPU), Edificio M5, Parque Científico, C/ Adaja 8, 37185 Villamayor, Salamanca, Spain (current affiliation)

DOI: [10.21105/joss.0XXXX](https://doi.org/10.21105/joss.0XXXX)

Software

- [Review](#) ↗
- [Repository](#) ↗
- [Archive](#) ↗

Editor: [Editor Name](#) ↗

Submitted: 01 January XXXX

Published: 01 January XXXX

License

Authors of papers retain copyright and release the work under a Creative Commons Attribution 4.0 International License ([CC BY 4.0](#)).

Summary

ESVM (ElectroStatic Vlasov-Maxwell) is a Vlasov-Maxwell Fortran 95 code, parallelized with OpenMP and using Python 3 for post-processing, that allows for the study of collisionless plasmas. A plasma is a set of charged particles consisting of electrons and ionized atoms whose quantity is sufficiently large to behave collectively through the long-distance electromagnetic fields they produce. It is thought that more than 99.9% of visible matter in the Universe is in Plasma state. Consisting in an ionized gas composed of very light electrons moving in between quasi-immobile positively charged ions on short time scale, any electrostatic field is rapidly screened over the so-called Debye screening distance (Debye & Hückel, 1923) in a collisionless plasma. On such a short time scale or in very diluted plasmas where the number of electrons in such Debye spheres can be assumed to be infinite, the plasma electron population is correctly described by the Vlasov equation (Vlasov, 1938). Besides its simplicity, the resulting Vlasov-Maxwell set of equations is extremely rich in Physics and its many applications range from Astrophysics and theoretical Plasma Physics to intense laser-matter interaction experiments and industrial plasmas. Many finite volume numerical advection schemes (Godunov, 1959) are implemented in the code in order to discretize the Vlasov equation, namely : - the donor-cell scheme i.e. the downwind / upwind scheme (R. Courant et al., 1952) depending on the advection direction in each phase-space cell, - the Lax-Wendroff scheme (Lax & Wendroff, 1960), - the Fromm scheme (Fromm, 1968), - the Beam-Warming scheme (Beam & Warming, 1976), - the Van Leer scheme (Van Leer, 1977), - the minmod scheme (Roe, 1986), - the superbee scheme (Roe, 1986) and - two Monotonic Upwind-centered Scheme for Conservation Laws (MUSCL) (van Leer, 1979) schemes MUSCL2 (Crouseilles & Filbet, 2004) and MUSCL1 (Duclos et al., 2009).

Contrary to the linear second order Lax-Wendroff, Fromm and Beam-Warming schemes, the non-linear second order minmod, superbee, Van Leer and MUSCL schemes make use of a Total Variation Diminishing (TVD) non-linear flux limiter with the price of becoming a first order scheme in some phase-space cells to limit the numerical oscillations. The donor-cell scheme is a first order method and has the pros of limiting such eventual oscillations but the cons of being numerically less consistent and more diffusive too. In ESVM, the discretized Vlasov equation is coupled with the self-consistent Maxwell-Gauss equation or equivalently with the Maxwell-Ampere equation with Maxwell-Gauss equation computed at the first time step, only. While the second order Maxwell-Gauss solver needs a computationally expensive inversion of a tridiagonal matrix for the computation of the Poisson equation, the Maxwell-Ampere equation solver makes use of the faster second order finite difference Yee scheme (Yee, 1966). Both absorbing and periodic boundary conditions for both the particles and the fields are implemented. Python scripts, using the Matplotlib and Numpy packages, are provided to automatically extract and plot the stored simulation results. Compilation rules can be easily

45 modified depending on the user compiler preferences using the provided makefile. It is however
 46 recommended to compile the code using the double-precision compiler option. Well known
 47 Plasma Physics academic cases, tools for testing the compilation and tools for checking the
 48 simulation parameters that are specified by the user in the input-deck are provided.

49 Statement of need

50 ESVM has been developed in order to adapt simulations to specific Plasma Physics problems
 51 by choosing the more adequate finite volume numerical advection scheme in order to compute
 52 the Vlasov equation phase-space advection derivatives and to choose between computing the
 53 Maxwell-Gauss equation or the Maxwell-Ampere equation with Maxwell-Gauss equation com-
 54 puted at the first time step, only. The code aims at being used by the open-source Highly
 55 Parallel Computing (HPC) Plasma Physics community ranging from under or post-graduate
 56 students to teachers and researchers who usually use Particle-In-Cell (PIC) codes (Dawson,
 57 1962) to study collisionless plasmas. Indeed, the PIC method may prohibit the study of
 58 Plasma Physical processes on large time scales and/or for very dense collisionless plasmas due
 59 to the statistical and numerical fluctuations of the computed quantities imposed by the use of
 60 a finite number of macroparticles. Also, plasma instabilities naturally develop in PIC codes,
 61 seeded by the available fluctuations spatial spectrum k -vector for which the instability growth
 62 rate is maximum and some small amplitude Plasma Physical processes may be hidden under
 63 the fluctuations level. Compared to the many open source PIC code such as (Derouillat et
 64 al., 2018) and semi-Lagrangian codes such as (de Buyl, 2014), there is no open source finite
 65 volume Vlasov codes in the literature that are not based on an expansion method such as
 66 (Tzoufras et al., 2011) (Touati et al., 2014) or (Joglekar & Levy, 2020). In addition, since
 67 the Vlasov equation is a conservation equation of the number of particle in the phase-space,
 68 using a finite volume method in order to compute the Vlasov equation presents the advantage
 69 of allowing for the use of numerical schemes that are numerically flux conserving and/or that
 70 ensure the distribution function positivity compared to other numerical methods. ESVM has
 71 already been used during courses for under and post-graduate students about the “numerical
 72 tools for laser-plasma interaction Physics” and it is currently used for theoretical Plasma
 73 Physics investigations.

74 Equations computed by ESVM

75 Plasma ions are assumed to be immobile with a homogeneous density n_i and fully ionized
 76 with an electrical charge Ze where Z is the plasma ion atomic number and e the elementary
 77 charge. The plasma electron distribution function $f_e(x, v_x, t)$ is computed by ESVM according
 78 to the plasma electron Vlasov equation

$$\frac{\partial f_e}{\partial t}(x, v_x, t) + \frac{\partial}{\partial x}(v_x f_e(x, v_x, t)) - \frac{\partial}{\partial v_x} \left(\frac{e}{m_e} E_x(x, t) f_e(x, v_x, t) \right) = 0 \quad (1)$$

79 that is self-consistently coupled with the Maxwell-Gauss equation

$$\frac{\partial E_x}{\partial x}(x, t) = 4\pi e (Zn_i - n_e(x, t)) \quad (2)$$

80 for the electrostatic field $E_x(x, t)$ or, equivalently, self-consistently coupled with the Maxwell-
 81 Ampere equation

$$\frac{\partial E_x}{\partial t}(x, t) = -4\pi j_e(x, t) \quad (3)$$

82 with Maxwell-Gauss equation Equation 2 computed at the simulation start $t = 0$, only. Indeed,
 83 by integrating the plasma electron Vlasov equation Equation 1 over the whole plasma electron

84 velocity space $v_x \in [v_{x,\min}, v_{x,\max}]$, one gets the hydrodynamic equation of plasma electron
85 number conservation

$$\frac{\partial n_e}{\partial t}(x, t) + \frac{\partial}{\partial x} (n_e v_e(x, t)) = 0, \quad (4)$$

86 which, when injected in the time derivative of Maxwell-Gauss equation Equation 2, provides
87 the Maxwell-Ampere equation Equation 3 if Maxwell-Gauss equation Equation 2 is verified at
88 the simulation start $t=0$. Here,

$$n_e(x, t) = \int_{v_{x,\min}}^{v_{x,\max}} f_e(x, v_x, t) dv_x, \quad (5)$$

89

$$v_e(x, t) = \frac{1}{n_e(x, t)} \int_{v_{x,\min}}^{v_{x,\max}} f_e(x, v_x, t) v_x dv_x \quad (6)$$

90 and

$$j_e(x, t) = -en_e(x, t)v_e(x, t) \quad (7)$$

91 are the plasma electron density, mean velocity and electrical charge current, respectively.
92 ESVM also computes the plasma electron thermal velocity $v_{T_e}(x, t)$ defined according to the
93 plasma electron internal energy density

$$u_{T_e}(x, t) = \frac{n_e(x, t)}{2} m_e v_{T_e}(x, t)^2 = \frac{m_e}{2} \int_{v_{x,\min}}^{v_{x,\max}} f_e(x, v_x, t) (v_x - v_e(x, t))^2 dv_x. \quad (8)$$

94 For example, in 1D plasmas at local Maxwell-Boltzmann equilibrium, $v_{T_e}(x, t) =$
95 $\sqrt{k_B T_e(x, t)/m_e}$ where k_B is the Boltzmann constant, $T_e(x, t)$ is the local electron
96 temperature and m_e the electron mass. Maxwell-Gauss equation Equation 2 is computed by
97 using the electrostatic potential definition

$$\frac{\partial \Phi}{\partial x}(x, t) = -E_x(x, t) \quad (9)$$

98 that gives the Poisson equation

$$\frac{\partial^2 \Phi}{\partial x^2}(x, t) = -4\pi e (Zn_i - n_e(x, t)) \quad (10)$$

99 for the electrostatic potential Φ when injected in the Maxwell-Gauss equation Equation 2.
100 When the simulation is running, ESVM stores at every time steps and displays on the terminal
101 at every dumped time steps t_d the total plasma electron internal and kinetic energy (assuming
102 simulations with an area unit perpendicular to the x -axis of λ_{Debye}^2) and the total electrostatic
103 energy in the simulation box $x \in [x_{\min}, x_{\max}]$

$$U_{T_e}(t_d) = \lambda_{\text{Debye}}^2 \int_{x_{\min}}^{x_{\max}} u_{T_e}(x, t_d) dx, \quad (11)$$

104

$$U_{K_e}(t_d) = \lambda_{\text{Debye}}^2 \int_{x_{\min}}^{x_{\max}} n_e(x, t) \frac{m_e v_e(x, t_d)^2}{2} dx \quad (12)$$

105 and

$$U_{E_x}(t_d) = \lambda_{\text{Debye}}^2 \int_{x_{\min}}^{x_{\max}} \frac{E_x(x, t_d)^2}{8\pi} dx, \quad (13)$$

106 respectively as well as the total energy area density

$$U_{\text{tot}}(t_d) = U_{T_e}(t_d) + U_{K_e}(t_d) + U_{E_x}(t_d) \quad (14)$$

107 in order to check the energy conservation in the simulation. The user can initialize : - an
108 initial plasma electron population at Maxwell-Boltzmann equilibrium drifting at the velocity v_d
109

$$\begin{cases} f_e(x, v_x, t = 0) &= \frac{Zn_i}{\sqrt{2\pi v_{Te_0}^2}} \exp\left[-\frac{(v_x - v_d)^2}{2v_{Te_0}^2}\right] \\ E_x(x, t = 0) &= 0 \end{cases} \quad (15)$$

110 by no imposing any perturbation parameter or - a well known Plasma Physics process;
111 cf. section **ESVM Plasma Physics academic case simulations**. - Finally, specific Plasma
112 Physics simulations can easily be added in ESVM by implementing them in the Fortran 95
113 subroutine INIT_SIMU of the library.f90 source file.

114 ESVM units

115 The code units consist in the commonly used electrostatic units : the electron mass m_e for
116 masses, the elementary charge e for electrical charges, the inverse of the Langmuir plasma
117 electron angular frequency $\omega_p = \sqrt{4\pi Zn_i e^2 / m_e}$ for times, the Debye electron screening length
118 $\lambda_{Debye} = v_{Te_0} / \omega_p$ and the constant electron density $n_0 = Zn_i$ for spatial densities. v_{Te_0} is
119 therefore an important unit parameter of normalization since it fixes indirectly the space unit.
120 It can be defined more generally as the initial plasma electron velocity distribution standard
121 deviation if the plasma is not initialized at Maxwell-Boltzmann thermodynamic equilibrium;
122 cf. Equation 8. Injecting these units in the equations computed by the code, one deduces the
123 resulting normalized electrostatic field and electron distribution function that consequently
124 reads $\underline{E}_x = eE_x / m_e \omega_p v_{Te_0}$ and $\underline{f}_e = f_e v_{Te_0} / n_0$, respectively.

125 ESVM numerical stability

126 The spatial grid cells should be chosen lower than the Debye length $\Delta x < \lambda_{Debye}$ for the
127 simulation to be Physical. $v_{x,min}$ and $v_{x,max}$ should be chosen sufficiently large $|v_{x,min/max}| \gg$
128 v_{Te_0} in such a way that there is no plasma electrons outside the simulation velocity space
129 during the whole simulation. The simulation velocity bin size should be chosen lower than
130 the thermal electron velocity $\Delta v_x < v_{Te_0}$ and also sufficiently small to capture the desired
131 Physics. The CFL stability condition (from the name of its finder R. Courant, K. Friedrichs
132 and H. Lewy (R. Courant et al., 1928)) is implemented inside the code in such a way that
133 the user just needs to specify in the input deck the scalar parameter $cfl < 1$ such that the
134 normalized simulation time step reads

$$\underline{\Delta t}_n = cfl \times F^n(\underline{\Delta x}, \underline{\Delta v}_x) < F^n(\underline{\Delta x}, \underline{\Delta v}_x) \quad (16)$$

135 at the time step $\underline{t}_n = \sum_{m=1}^n \underline{\Delta t}_m$ at time iteration n where $F^n(\underline{\Delta x}, \underline{\Delta v}_x)$ depends on the
136 chosen numerical scheme.

137 For example, if one notes

$$\underline{f}_e^{n,i} = \frac{1}{\underline{\Delta x}} \int_{\underline{x}_{i-1/2}}^{\underline{x}_{i+1/2}} \underline{f}_e(\underline{x}, \underline{t}_n) d\underline{x} \quad (17)$$

138 the electron distribution function finite volume at the spatial location \underline{x}_i located in between
139 $\underline{x}_{i-1/2} = \underline{x}_i - \underline{\Delta x}/2$ and $\underline{x}_{i+1/2} = \underline{x}_i + \underline{\Delta x}/2$ and one considers the Lax-Wendroff method
140 to compute the advection

$$\frac{\partial \underline{f}_e}{\partial \underline{t}} + \underline{v}_x \frac{\partial \underline{f}_e}{\partial \underline{x}} = 0 \quad (18)$$

of plasma electrons along the spatial \underline{x} -axis in the phase-space, the numerical scheme reads

$$\left[\frac{f_e^{n+1} - f_e^n}{\Delta t_n} \right]^i + v_x \left[\frac{F_x^{i+1/2} - F_x^{i-1/2}}{\Delta x} \right]^n = 0 \quad (19)$$

where the plasma electron fluxes across the volume sections located at $\underline{x}_{i\pm 1/2}$ are given by

$$F_x^{n,i+1/2} = \frac{f_e^{n,i+1} + f_e^{n,i}}{2} - \frac{v_x \Delta t_n}{\Delta x} \frac{f_e^{n,i+1} - f_e^{n,i}}{2} \quad (20)$$

and

$$F_x^{n,i-1/2} = \frac{f_e^{n,i} + f_e^{n,i-1}}{2} - \frac{v_x \Delta t_n}{\Delta x} \frac{f_e^{n,i} - f_e^{n,i-1}}{2}. \quad (21)$$

According to the Taylor expansion of $f_e^{n,i+i}$, $f_e^{n,i-i}$ and $f_e^{n+1,i}$ close to (\underline{x}_i, t_n) up to the third order in space and time, one can check the Lax-Wendroff numerical consistency error is indeed of second order :

$$\begin{aligned} \epsilon^{n,i} &= \left[\frac{f_e^{n+1} - f_e^n}{\Delta t_n} \right]^i + v_x \left[\frac{F_x^{i+1/2} - F_x^{i-1/2}}{\Delta x} \right]^n - \left(\frac{\partial f_e}{\partial t} \Big|^{n,i} + v_x \frac{\partial f_e}{\partial x} \Big|^{n,i} \right) \\ &= \frac{\Delta t_n^2}{6} \frac{\partial^3 f_e}{\partial t^3} \Big|^{n,i} + v_x \frac{\Delta x^2}{6} \frac{\partial^3 f_e}{\partial x^3} \Big|^{n,i} + O(\Delta t_n^3 + \Delta x^3 + \Delta t_n \Delta x^2). \end{aligned} \quad (22)$$

By using the Von Neumann stability analysis, assuming periodic boundary conditions for simplicity and noting

$$\hat{f}_e^n(\underline{k}^p) = \frac{1}{N_x} \sum_{i=1}^{N_x} f_e^{i,n} \exp(-i \underline{k}^p \underline{x}_i) \Leftrightarrow f_e^{n,i} = \sum_{p=1}^{N_x} \hat{f}_e^n(\underline{k}^p) \exp(i \underline{k}^p \underline{x}_i) \quad (23)$$

with $\ell^2 = -1$, $N_x = 1 + (\underline{x}_{\max} - \underline{x}_{\min})/\Delta x$ the number of spatial grid points and $\underline{k}^p = 2\pi(p-1)/(\underline{x}_{\max} - \underline{x}_{\min})$ the discrete Fourier mode, one gets by injecting Equation 23 in Equation 19

$$\frac{\hat{f}_e^{n+1}(\underline{k}^p)}{\hat{f}_e^n(\underline{k}^p)} = 1 - \frac{v_x \Delta t_n}{\Delta x} \ell \sin(\underline{k}^p \Delta x) + \left(\frac{v_x \Delta t_n}{\Delta x} \right)^2 [\cos(\underline{k}^p \Delta x) - 1] \quad (24)$$

for each term p of the series. It implies the numerical scheme is stable,

$$\text{meaning } \left| \frac{\hat{f}_e^{n+1}(\underline{k}^p)}{\hat{f}_e^n(\underline{k}^p)} \right| < 1, \text{ if } \Delta t_n < \frac{\Delta x}{v_x}. \quad (25)$$

Performing the same reasoning when discretizing also the velocity space $\underline{v}_x^\ell = \underline{v}_{x,\min} + (\ell - 1)\Delta v_x$ with $N_{v_x} = 1 + (v_{x,\max} - v_{x,\min})/\Delta v_x$ velocity grid points and considering in addition the advection term of plasma electrons along the \underline{v}_x -axis in the velocity space for computing the Vlasov equation Equation 1 with each numerical scheme implemented in ESVM, one finds (sometimes empirically when it is too difficult analytically) that

$$F^n(\Delta x, \Delta v_x) = \frac{1/2}{\frac{\max_{\ell \in [1, N_{v_x}]} \{v_x^\ell\}}{\Delta x} + \frac{\max_{i \in [1, N_x]} \{E_x^{n,i}\}}{\Delta v_x}}. \quad (26)$$

is a sufficient CFL stability condition for all numerical schemes implemented in ESVM to be stable.

ESVM Plasma Physics academic case simulations

Four well-known Plasma Physics academic cases are provided with ESVM : 1) the emission of an electrostatic wakefield by a Gaussian electron; cf. Figure 1 2) the linear Landau damping of an electron plasma wave; cf. Figure 2, 3) the non-linear Landau damping of an electron plasma wave; cf. Figure 3 and 4) the two-stream instability of two counter-propagating symmetric Gaussian electron beams; cf. Figure 4.

For each academic case, an example of input deck is provided together with the corresponding simulation result plots that the code typically generates. For 1), 2) and 3), the simulation is initialized assuming a non-drifting collisionless plasma at Maxwell-Boltzmann equilibrium

$$\begin{cases} f_e^{(0)}(x, v_x, t = 0) &= \frac{Zn_i}{\sqrt{2\pi v_{Te_0}^2}} \exp\left[-\frac{v_x^2}{2v_{Te_0}^2}\right] \\ E_x^{(0)}(x, t = 0) &= 0 \end{cases} \quad (27)$$

that is perturbed : - with a small perturbation

$$\delta f_e(x, v_x, t = 0) = A \frac{Zn_i}{2\pi\delta x\delta v} \exp\left[-\frac{(x - x_d)^2}{2\delta x^2}\right] \exp\left[-\frac{(v_x - v_d)^2}{2\delta v^2}\right], \quad (28)$$

consisting in a Gaussian electron located at $x_d = x_{\min} + (x_{\max} - x_{\min})/8$ with a standard deviation $\delta x = \lambda_{\text{Debye}}/4$ and drifting at a velocity v_d with a standard deviation $\delta v = v_{Te_0}/40$ at the simulation start $t = 0$ for 1), and - with a small perturbation consisting in a small amplitude electron plasma wave

$$\delta E_x(x, t < \delta t) = A \frac{m_e \omega_p v_{Te_0}}{e} \sin(\omega_0 t - kx) \quad (29)$$

propagating during a short time interval $\delta t = 6\pi/\omega_0$ after the simulation start $t = 0$ for 2) and 3).

Only the perturbation amplitudes $A < 1$ for 1), 2) and 3), the perturbation drift velocity $v_d > v_{Te_0}$ for 1) and the perturbation temporal and spatial angular frequencies ω_0 and k for 2) and 3) should be modified by the user when filling the input-deck in such a way that

$$\begin{cases} f_e(x, v_x, t) &= f_e^{(0)}(x, v_x, t) + \delta f_e(x, v_x, t) \\ E_x(x, t) &= E_x^{(0)}(x, t) + \delta E_x(x, t) \end{cases} \quad \text{with } |\delta f_e(x, v_x, t)| \ll f_e^{(0)}(x, v_x, t) \quad (30)$$

keeps being respected during the linear stage of the simulation. Except for non-linear Plasma Physics processes such as 3) for which the non-linear theory should be considered, the methodology that can be used to check any ESVM simulation results is always the same. Only analytical estimates used to check the ESVM simulation results of the provided academic case 4) are consequently detailed here in order to highlight it. The user can check the provided academic case simulation results 1), 2) and 3) by directly comparing the ESVM simulation results with the analytical estimates provided in (Decyk, 1987) (available at <https://picksc.idre.ucla.edu/wp-content/uploads/2015/04/DecykKyiv1987.pdf>) and in the reference textbooks (Landau & Lifshitz, 1981) and (Sagdeev & Galeev, 1969), respectively.

The provided Plasma Physics academic case 4) is initialized assuming two counter-propagating homogeneous Gaussian electron beams 'e, +' and 'e, -' of exactly opposite drift velocity $\pm v_d$ with same standard velocity deviation v_{Te_0}

$$f_e^{(0)}(x, v_x, t) = f_{e,+}^{(0)}(x, v_x, t) + f_{e,-}^{(0)}(x, v_x, t) \quad (31)$$

with

$$f_{e,\pm}^{(0)}(x, v_x, t) = \frac{Zn_i/2}{\sqrt{2\pi v_{Te_0}^2}} \exp\left[-\frac{(v_x \mp v_d)^2}{2v_{Te_0}^2}\right] \quad (32)$$

192 that is a solution of the Vlasov Equation Equation 1 and that doesn't produce any electrostatic
193 fields

$$E_x^{(0)}(x, t) = 0 \quad (33)$$

194 according to Maxwell-Gauss Equation Equation 2. If one computes the Vlasov-Maxwell set
195 of Equations {Equation 1, Equation 2} exactly, initializing it with the two-stream equilibrium
196 distribution function Equation 31 without any perturbation, the counter-propagating elec-
197 tron beams would continue their propagation through the immobile plasma ions without any
198 modification. In order to observe the two-stream instability,

$$f_e(x, v_x, t = 0) = f_e^{(0)}(x, v_x, t = 0) + \delta f_e(x, v_x, t = 0), \quad (34)$$

199 is initialized instead by adding a small perturbation

$$\delta f_e(x, v_x, t = 0) = \delta f_{e,+}(x, v_x, t = 0) + \delta f_{e,-}(x, v_x, t = 0) \quad (35)$$

200 on each beam of the form

$$\delta f_{e,\pm}(x, v_x, t = 0) = \pm A \sin(k_1 x) f_{e,\pm}^{(0)}(x, v_x, t = 0) \quad (36)$$

201 at the simulation start $t = 0$ with $A = 0.1$, $k_1 = 2\pi/L_x$ (parameter k in the input-deck)
202 where $L_x = x_{\max} - x_{\min}$ can be modified by the user in the input-deck.

203 In order to get analytical estimates of growing plasma electron density and mean velocity and
204 electrostatic fields in this ESVM simulation, one can linearize the Vlasov equation Equation 1
205 and the self-consistent Maxwell-Gauss equation Equation 2 computed by ESVM assuming the
206 perturbation Equation 35 remains small compared to the equilibrium distribution Equation 31
207 during the simulation. They read

$$\frac{\partial \delta f_e}{\partial t} + \frac{\partial}{\partial x}(v_x \delta f_e) - \frac{e}{m_e} \frac{df_e^{(0)}}{dv_x} \delta E_x = 0 \quad (37)$$

208 and

$$\frac{\partial \delta E_x}{\partial x} = -4\pi e \int_{-\infty}^{\infty} \delta f_e dv_x, \quad (38)$$

209 up to the first order. Considering periodic boundary conditions, we may use a one-sided
210 Fourier transformation in time (thus equivalent to a Laplace transform) and a Fourier series
211 expansion in space for such a L_x -periodic initial condition problem. We will note

$$\hat{X}_p(t) = \frac{1}{L_x} \int_0^{L_x} X(x, t) \exp(+ik_p x) dx \Leftrightarrow X(x, t) = \sum_{p=-\infty}^{\infty} \hat{X}_p(t) \exp(-ik_p x) \quad (39)$$

212 with $\forall p \in \mathbb{Z}$, $k_p = 2\pi p/L_x$ and

$$\begin{aligned} \hat{\hat{X}}_p^{(+)}(\omega) &= \int_0^{\infty} dt \hat{X}_p(t) \exp(-i\omega t) \\ &= \int_0^{\infty} dt \int_0^{L_x} \frac{dx}{L_x} X(x, t) \exp[-i(\omega t - k_p x)] \\ \Leftrightarrow X(x, t) &= \int_{iR-\infty}^{iR+\infty} \frac{d\omega}{2\pi} \sum_{p=-\infty}^{\infty} \hat{\hat{X}}_p^{(+)}(\omega) \exp[+i(\omega t - k_p x)] \end{aligned} \quad (40)$$

213 where the integral in the complex ω -plane is taken along a straight line $\omega = iR$. By multiplying
214 Equation 37 and Equation 38 by $\exp[-i(\omega t - k_p x)]/L_x$ and by integrating them from $x =$
215 $-\infty$ to $x = \infty$ and from $t = 0$ to $t = \infty$, we obtain respectively

$$\hat{\hat{f}}_{e,p}^{(+)} = \frac{1}{i(\omega - k_p v_x)} \left[\hat{\hat{f}}_{e,p}(v_x, t = 0) + \frac{e}{m_e} \frac{df_e^{(0)}}{dv_x} \hat{\hat{E}}_{x,p}^{(+)} \right] \quad (41)$$

216 with

$$\widehat{\delta f}_{e,p}(v_x, t=0) = \alpha_p A \frac{Z n_i / 2}{\sqrt{2\pi v_{Te_0}^2}} \left\{ \exp \left[-\frac{(v_x - v_d)^2}{2v_{Te_0}^2} \right] - \exp \left[-\frac{(v_x + v_d)^2}{2v_{Te_0}^2} \right] \right\} \quad (42)$$

217 where

$$\alpha_p = \begin{cases} \mp 1/2\iota & \text{if } p = \pm 1 \\ 0 & \text{else} \end{cases} \quad (43)$$

218 and

$$\widehat{\delta E}_{x,p}^{(+)} = \frac{4\pi e}{\iota k_p} \int_{-\infty}^{\infty} \widehat{\delta f}_{e,p}^{(+)}(\omega, v_x) dv_x. \quad (44)$$

219 Injecting Equation 41 in Equation 44, we obtain the Fourier components of the electrostatic
220 field Laplace transform

$$\begin{aligned} \widehat{\delta E}_{x,p}^{(+)}(\omega) &= \frac{4\pi e}{k_p^2 \epsilon(\omega, k_p)} \int_{-\infty}^{\infty} \frac{\widehat{\delta f}_{e,p}(v_x, t=0)}{v_x - \omega/k_p} dv_x \\ &= \alpha_p \frac{A}{2\sqrt{2}} \frac{m_e v_{Te_0}}{e} \frac{Z \left(\frac{\omega/k_p - v_d}{v_{Te_0} \sqrt{2}} \right) - Z \left(\frac{\omega/k_p + v_d}{v_{Te_0} \sqrt{2}} \right)}{\epsilon(\omega, k_p) (k_p \lambda_{\text{Debye}})^2} \end{aligned} \quad (45)$$

221 where the plasma electrical permittivity reads

$$\begin{aligned} \epsilon(\omega, k) &= 1 - \frac{4\pi e^2}{m_e k^2} \int_{-\infty}^{\infty} \frac{1}{v_x - \omega/k} \frac{df_e^{(0)}}{dv_x} dv_x \\ &= 1 + \frac{1}{(k \lambda_{\text{Debye}})^2} \left\{ 1 + \frac{1}{2} \left[F \left(\frac{\omega/k - v_d}{v_{Te_0} \sqrt{2}} \right) + F \left(\frac{\omega/k + v_d}{v_{Te_0} \sqrt{2}} \right) \right] \right\} \end{aligned} \quad (46)$$

222 depending on the plasma dispersion function (Fried & Conte, 1961)

$$F(\zeta) = \zeta Z(\zeta) \text{ and } Z(\zeta) = \frac{1}{\sqrt{\pi}} \int_{-\infty}^{\infty} \frac{\exp(-z^2)}{z - \zeta} dz. \quad (47)$$

223 Since $v_d \gg v_{Te_0}$ in this ESVM simulation, we have the condition

$$\left| \frac{\omega}{k_p} \pm v_d \right| \gg v_{Te_0} \sqrt{2} \quad (48)$$

224 that is fulfilled for any given spatial frequency mode k_p and one thus may use the asymptotic
225 limit

$$F(\zeta) \underset{|\zeta| \gg 1}{=} \iota \zeta \sqrt{\pi} \exp(-\zeta^2) - 1 - \frac{1}{2\zeta^2} - \frac{3}{4\zeta^4} + O\left(\frac{1}{\zeta^6}\right) \quad (49)$$

226 that leads to the simpler dispersion relation

$$\epsilon(\omega, k) \underset{v_d \gg v_{Te_0}}{=} 1 - \frac{\omega_p^2}{2} \left[\frac{1}{(\omega - kv_d)^2} + \frac{1}{(\omega + kv_d)^2} \right] = 0 \quad (50)$$

227 retaining only the main term in the series expansion of the dispersion function Equation 47
228 up to the second order Equation 49. In this limit, the dispersion relation Equation 50 provides
229 four pure real solutions $\{\omega_1(k), \omega_2(k), \omega_3(k), \omega_4(k)\} \in \mathbb{R}^4$ for wavenumber k greater
230 or equal than the critical wavenumber ω_p/v_d . It means that the two counter-propagating
231 electron beams remain stable on space scales smaller than $2\pi v_d/\omega_p$. However, in the case
232 where $k_p < \omega_p/v_d$ considered here, one finds in addition to the two real poles

$$\omega_{1/2} \left(k < \frac{\omega_p}{v_d} \right) = \pm \omega_0(k) \quad (51)$$

233 where

$$\omega_0(k) = \omega_p \sqrt{\left(\frac{kv_d}{\omega_p}\right)^2 + \frac{1}{2} \left(1 + \sqrt{1 + 8\left(\frac{kv_d}{\omega_p}\right)^2}\right)} \underset{kv_d \ll \omega_p}{\sim} \omega_p, \quad (52)$$

234 two another pure imaginary conjugate poles

$$\omega_{3/4}(k < k_c) = \pm i\delta(k). \quad (53)$$

235 It means that the two counter-propagating electron beams streaming throught the immobile
236 plasma ions are unstable on space scales greater than $2\pi v_d/\omega_p$ and that this two-stream
237 instability grows exponentially at the rate

$$\delta(k) = \omega_p \sqrt{\frac{1}{2} \left(\sqrt{1 + 8\left(\frac{kv_d}{\omega_p}\right)^2} - 1 \right) - \left(\frac{kv_d}{\omega_p}\right)^2} \underset{kv_d \ll \omega_p}{\sim} |k| v_d. \quad (54)$$

238 The stable electron plasma waves angular frequency [Equation 52](#) and the two stream instability
239 growth rate [Equation 54](#) are plotted in [Figure 5](#) as a function of the angular spatial frequency
240 mode k . Retaining the main terms in the series expansions of \mathcal{Z} up to the second order
241 in [Equation 45](#) according to [Equation 49](#), the Fourier components of the electrostatic field
242 Laplace transform simplify into

$$\widehat{\widehat{\mathbf{E}}}_{x,p}^{(+)}(\omega) \underset{v_d \gg v_{Te0}}{\sim} -\alpha_p A \frac{m_e v_d}{e} \frac{\omega_p^2}{\epsilon(\omega, k_p)(\omega - k_p v_d)(\omega + k_p v_d)}. \quad (55)$$

243 The poles of the Fourier components of the electrostatic fields [Equation 55](#) are thus $\pm k_p v_d$
244 plus the ones of the plasma electrical permittivity [Equation 50](#) given by [Equations 51](#) and
245 [Equation 53](#). We can now determine the time dependance of the spatial Fourier components
246 of the growing electrostatic field

$$\widehat{\widehat{\mathbf{E}}}_{x,p}(t) = \frac{1}{2\pi} \int_{\iota R - \infty}^{\iota R + \infty} \widehat{\widehat{\mathbf{E}}}_{x,p}^{(+)}(\omega) \exp(+i\omega t) d\omega \quad (56)$$

247 by using the residue theorem with the contour illustrated in [Figure 6](#) in order to evaluate
248 the Cauchy principal value of this integral : since the function to integrate in [Equation 56](#)
249 is an analytic function of ω defined in the whole complex plane, we moved the contour of
250 integration usually taken slightly above the real axis into the lower half-plane sufficiently far
251 beneath the pole $-i\delta$ and passing round this pole and round the other poles lying above it in
252 such a way that it doesn't cross any of the poles of the function. We thus obtain

$$\begin{aligned} \widehat{\widehat{\mathbf{E}}}_{x,p}(t) &= A \frac{E_0}{2} \alpha_p \frac{\omega_p}{\omega_0(k_p)} \frac{\delta(k_p)^2 + (k_p v_d)^2}{\delta(k_p)^2 + \omega_0(k_p)^2} \sinh[\delta(k_p)t] \\ &+ A \frac{E_0}{2} \alpha_p \frac{\omega_p}{\omega_0(k_p)} \frac{\omega_0(k_p)^2 - (k_p v_d)^2}{\delta(k_p)^2 + \omega_0(k_p)^2} \sin[\omega_0(k_p)t] \end{aligned} \quad (57)$$

253 with

$$E_0 = \frac{m_e v_d \omega_p}{e} \quad (58)$$

254 that finally gives according to the Fourier series expansion [Equation 39](#)

$$\begin{aligned} \delta E_x(x, t) &= A \frac{E_0}{2} \alpha_p \frac{\omega_p}{\omega_0(k_1)} \frac{\delta(k_1)^2 + (k_1 v_d)^2}{\delta(k_1)^2 + \omega_0(k_1)^2} \sinh[\delta(k_1)t] \sin(k_1 x) \\ &+ A \frac{E_0}{2} \alpha_p \frac{\omega_p}{\omega_0(k_1)} \frac{\omega_0(k_1)^2 - (k_1 v_d)^2}{\delta(k_1)^2 + \omega_0(k_1)^2} \sin[\omega_0(k_1)t] \sin(k_1 x). \end{aligned} \quad (59)$$

255 Knowing the electrostatic field Equation 59, one may also deduce the perturbed distribution
256 function according to Equation 37. It reads

$$\begin{aligned}\delta f_e(x, v_x, t) &= \delta f_e(x, v_x, t=0) + \frac{e}{m_e} \frac{df_e^{(0)}}{dv_x}(v_x) \int_0^t \delta E_x[x + v_x(\tau - t), \tau] d\tau \\ &= f_{e,+}^{(0)}(v_x) \left[A \sin(k_1 x) + \frac{v_d - v_x}{v_{Te0}^2} \frac{e}{m_e} \int_0^t \delta E_x[x + v_x(\tau - t), \tau] d\tau \right] \\ &+ f_{e,-}^{(0)}(v_x) \left[-A \sin(k_1 x) - \frac{v_d + v_x}{v_{Te0}^2} \frac{e}{m_e} \int_0^t \delta E_x[x + v_x(\tau - t), \tau] d\tau \right].\end{aligned}\quad (60)$$

257 In the limit $k_p v_d \ll \omega_p$, they simplify into

$$\delta E_x(x, t) \underset{k_1 v_d \ll \omega_p}{\sim} A \frac{E_0}{2} \left[\sin(\omega_p t) + 4 \frac{k_1 v_d}{\omega_p} \sinh(k_1 v_d t) \right] \sin(k_1 x) \quad (61)$$

258 and

$$\begin{aligned}\underset{k_1 v_d \ll \omega_p}{\sim} & A \frac{v_d}{1 - \left(\frac{k_1 v_x}{\omega_p}\right)^2} \left\{ \frac{e}{m_e} \int_0^t \delta E_x[x + v_x(\tau - t), \tau] d\tau \right. \\ & \left. \left\{ \frac{k_1 v_x}{\omega_p} \sin(\omega_p t) \cos(k_1 x) - [\cos(\omega_p t) - 1] \sin(k_1 x) \right\} \right\} \\ + & A \frac{v_d}{1 + \left(\frac{v_x}{v_d}\right)^2} \left\{ -\frac{v_x}{v_d} \sinh(k_1 v_d t) \cos(k_1 x) + [\cosh(k_1 v_d t) - 1] \sin(k_1 x) \right\}.\end{aligned}\quad (62)$$

259 We thus deduce in this limit

$$\begin{aligned}\delta n_e(x, t) &= \int_{-\infty}^{\infty} \delta f_e(x, v_x, t) dv_x \\ \underset{k_1 v_d \ll \omega_p}{\sim} & -\frac{A}{2} Z n_i \frac{k_1 v_d}{\omega_p} \left[\sin(\omega_p t) + 4 \frac{k_1 v_d}{\omega_p} \sinh(k_1 v_d t) \right] \cos(k_1 x)\end{aligned}\quad (63)$$

260 and

$$\begin{aligned}\delta v_e(x, t) &= \frac{1}{Z n_i} \int_{-\infty}^{\infty} v_x \delta f_e(x, v_x, t) dv_x \\ \underset{k_1 v_d \ll \omega_p}{\sim} & -\frac{A}{2} v_d \left[(\cos(\omega_p t) - 1) + \left(2 \frac{k_1 v_d}{\omega_p}\right)^2 (\cosh(k_1 v_d t) - 1) \right] \sin(k_1 x).\end{aligned}\quad (64)$$

261 The first term in the square brackets

$$\begin{cases} \delta n_{osc}(x, t) \underset{k_1 v_d \ll \omega_p}{\sim} -\frac{A}{2} Z n_i \frac{k_1 v_d}{\omega_p} \sin(\omega_p t) \cos(k_1 x) \\ \delta v_{osc}(x, t) \underset{k_1 v_d \ll \omega_p}{\sim} -\frac{A}{2} v_d (\cos(\omega_p t) - 1) \sin(k_1 x) \\ \delta E_{osc}(x, t) \underset{k_1 v_d \ll \omega_p}{\sim} \frac{A}{2} E_0 \sin(\omega_p t) \sin(k_1 x) \end{cases} \quad (65)$$

262 corresponds to space-charge oscillations of stationary electrostatic plasma waves excited by
263 the perturbation imposed on each electron beam. We are rather interested here in the second
264 term in the square brackets

$$\begin{cases} \delta n_{ins}(x, t) \underset{k_1 v_d \ll \omega_p}{\sim} -2A Z n_i \left(\frac{k_1 v_d}{\omega_p}\right)^2 \sinh(k_1 v_d t) \cos(k_1 x) \\ \delta v_{ins}(x, t) \underset{k_1 v_d \ll \omega_p}{\sim} -2A v_d \left(\frac{k_1 v_d}{\omega_p}\right)^2 (\cosh(k_1 v_d t) - 1) \sin(k_1 x) \\ \delta E_{ins}(x, t) \underset{k_1 v_d \ll \omega_p}{\sim} 2A E_0 \frac{k_1 v_d}{\omega_p} \sinh(k_1 v_d t) \sin(k_1 x) \end{cases} \quad (66)$$

corresponding to the exponentially growing electrostatic field due to the two-stream instability. These latter growing electron density, current density and electrostatic field perturbations Equation 66 can directly be compared with the ESVM simulation result. One can also check that if $A = 0$, all quantities cancel. That confirms that, contrary to PIC codes, the two counter-propagating electron beams would continue their propagation without any modification if we do not impose an initial perturbation on which the instability will grow in ESVM. Finally, one can estimate the trajectories (x_ℓ, v_ℓ) of one beam electron $\ell \in [1, N_e]$ with an arbitrary initial velocity $v_\ell(t=0) = v_0$ in the beam velocity distribution function and an initial position $x_\ell(t=0) = x_0$ close to $x = 0$ such that $k_1 x_0 \ll 1$. At the early stage of the instability, the growing electrostatic field component δE_{ins} is small compared to the stationary plasma wave δE_{osc} that oscillates in time at the Langmuir electron angular frequency ω_p . On such time scale $\omega_p t \sim 1$, the beam electrons are consequently mainly affected by this electrostatic field component

$$m_e \frac{dv_\ell}{dt} = -e\delta E_{\text{osc}}(x_\ell(t), t) \quad (67)$$

and their trajectory is thus given by

$$\frac{d^2 x_\ell}{dt^2} + \omega_p^2 \left(\frac{A k_1 v_d}{2 \omega_p} \right) \sin(\omega_p t) x_\ell(t) = 0, \quad (68)$$

assuming that $k_1 x_\ell(t) \ll 1$ remains valid at every time $t > 0$ if it is valid at $t = 0$ such that $\forall t, \sin[k_1 x_\ell(t)] \sim k_1 x_\ell(t)$. Recognizing the Mathieu Equation

$$\frac{d^2 x_\ell}{du^2} + [a - 2q \cos(2u)] x_\ell(u) = 0 \quad (69)$$

with $a = 0$ and $q = -Ak_1 v_d / \omega_p$ by doing the change of variable $u(t) = (-\pi/4) + (\omega_p t/2)$, we deduce

$$k_1 x_\ell(t) = k_1 x_c c_{e,0}[q, u(t)] + k_1 x_s s_{e,0}[q, u(t)] \quad (70)$$

and

$$v_\ell(t) = \frac{v_d}{2} \frac{\omega_p}{k_1 v_d} \{k_1 x_c c'_{e,0}[q, u(t)] + k_1 x_s s'_{e,0}[q, u(t)]\} \quad (71)$$

with

$$\begin{cases} k_1 x_c = + \frac{s'_{e,0}(q, -\pi/4) k_1 x_0 - s_{e,0}(q, -\pi/4) (2k_1 v_d / \omega_p) (v_0 / v_d)}{c_{e,0}(q, -\pi/4) s'_{e,0}(q, -\pi/4) - c'_{e,0}(q, -\pi/4) s_{e,0}(q, -\pi/4)} \\ k_1 x_s = - \frac{c'_{e,0}(q, -\pi/4) k_1 x_0 - c_{e,0}(q, -\pi/4) (2k_1 v_d / \omega_p) (v_0 / v_d)}{c_{e,0}(q, -\pi/4) s'_{e,0}(q, -\pi/4) - c'_{e,0}(q, -\pi/4) s_{e,0}(q, -\pi/4)} \end{cases}, \quad (72)$$

accounting for the initial conditions at $t = 0$. Here, $c_{e,a}(q, u)$ and $s_{e,a}(q, u)$ are respectively the even and odd solutions of Mathieu Equation Equation 69 and $c'_{e,a}(q, u)$ and $s'_{e,a}(q, u)$ their first order derivatives. According to Equation 70 and Equation 71, the beam electron trajectories in space are only slightly modified compared to their ballistic initial trajectory $x_0 + v_0 t$ with a velocity that oscillates around their initial value v_0 with amplitudes slightly increasing with time. As a consequence, each beam velocity dispersion slightly increases with its propagation distance until the growing component of the electrostatic field δE_{ins} becomes greater than δE_{osc} . When this occurs, the equation of motion

$$m_e \frac{dv_\ell}{dt} = -e\delta E_{\text{ins}}(x_\ell(t), t) \quad (73)$$

gives

$$\frac{1}{2} \left(\frac{v_\ell(t)}{v_d} \right)^2 - \frac{1}{2} \left(\frac{v_0}{v_d} \right)^2 = -2Ak_1 \int_0^t v_\ell(t) \sin[k_1 x_\ell(t)] \sinh(k_1 v_d t) dt \quad (74)$$

and

$$\frac{d^2 x_\ell}{dt^2} + 2k_1 v_d^2 \sinh(k_1 v_d t) \sin[k_1 x_\ell(t)] = 0. \quad (75)$$

The energy conservation Equation Equation 74 shows that, at the early stage of the instability, electrons having a positive velocity $v_\ell(t) > 0$ at a location $0 < x_\ell(t) < L_x/2$ as well as electrons having a negative velocity $v_\ell(t) < 0$ at a location $-L_x/2 < x_\ell(t) < 0$ are losing energy contrary to electrons having a negative velocity $v_\ell(t) < 0$ at a location $0 < x_\ell(t) < L_x/2$ or electrons having a positive velocity $v_\ell(t) > 0$ at a location $-L_x/2 < x_\ell(t) < 0$ that are earning energy. In order to determine such an electron trajectory according to its equation of motion Equation 75, one can assume in addition that $k_1 x_\ell(t) \ll 1$ remains valid at every time $t > 0$ if it is valid at $t = 0$ such that $\forall t, \sin[k_1 x_\ell(t)] \sim k_1 x_\ell(t)$ and consider time scales of the order of electrostatic plasma oscillations ω_p^{-1} so that we may consider $\sinh(k_1 v_d t) \sim \exp(k_1 v_d t)/2$. In this case, Equation 75 simplifies into

$$\frac{d^2 x_\ell}{dt^2} + (k_1 v_d)^2 \exp(k_1 v_d t) x_\ell(t) = 0. \quad (76)$$

Recognizing the differential Bessel Equation by doing the change of variable $v(t) = \exp(k_1 v_d t)$

$$\frac{d^2 x_\ell}{dv^2} + \frac{1}{v} \frac{dx_\ell}{dv} + \frac{1}{v} x_\ell(v) = 0, \quad (77)$$

the beam electron trajectories can be found readily. They read

$$k_1 x_\ell(t) = k_1 x_J J_0(2\sqrt{v(t)}) + k_1 x_Y Y_0(2\sqrt{v(t)}) \quad (78)$$

and

$$v_\ell(t) = -v_d \left[k_1 x_J J_1(2\sqrt{v(t)}) + k_1 x_Y Y_1(2\sqrt{v(t)}) \right] \sqrt{v(t)} \quad (79)$$

with

$$\begin{cases} k_1 x_J = + \frac{Y_1(2) k_1 x_0 + Y_0(2) (v_0/v_d)}{J_0(2) Y_1(2) - J_1(2) Y_0(2)} \\ k_1 x_Y = - \frac{J_1(2) k_1 x_0 + J_0(2) (v_0/v_d)}{J_0(2) Y_1(2) - J_1(2) Y_0(2)} \end{cases}, \quad (80)$$

accounting for the initial conditions at $t = 0$. Here, J_μ and Y_μ are the Bessel functions of the first and second kind of order μ respectively. Some of these beam electron orbits are plotted in Figure 7. We can see that the beam electrons are looping around the phase-space center $(x, v) = (0, 0)$ with a velocity amplitude increasing with their initial spatial distance from $x = 0$ in agreement with the ESVM simulation Figure 4.

ESVM Perspectives

It is planned in a near future to : 1) provide another Plasma Physics academic simulation about one BGK (from the name of its finder I. B. Bernstein, J. M. Greene and M. D. Kruskal) non linear electron plasma wave (Bernstein et al., 1957) 2) provide another Plasma Physics academic simulation about Plasma wave echo (Gould et al., 1967) 3) implement non-equally spaced phase-space cells 4) implement high order Weighted Essentially Non-Oscillatory (WENO) advection schemes (Liu et al., 1994) 5) compute the plasma ion Vlasov equation to allow for the ions to be mobile 6) implement MPI parallelization 7) implement vectorization 8) store the simulation results in hdf5 files instead of text files 9) extend the code to the relativistic regime : ESVM \Rightarrow RESVM for open source Relativistic ElectroStatic Vlasov-Maxwell code 10) implement a BGK (from the name of its finder P. L. Bhatnagar, E. P. Gross and M. Krook) collision operator (Bhatnagar et al., 1954) 11) extend the code to 1D-2V and 1D-3V phase-space electrostatic plasma simulations 12) implement the Landau (Landau, 1937) and Belaiev-Budker (Belaiev & Budker, 1956) relativistic collision operators using the Rosenbluth potentials (Rosenbluth et al., 1957) and their relativistic Braams-Karney extension (Braams & Karney, 1987) : (R)ESVM \Rightarrow (R)EMVFPM for open source (Relativistic) ElectroMagnetic Vlasov-Fokker-Planck-Maxwell code 13) extend the code to electromagnetic 2D-1V, 2D-2V and 2D-3V phase-space electrostatic electromagnetic plasma simulations

333 : (R)ESVM/(R)EMVM \Rightarrow (R)ESVM2/(R)EMVM2 and (R)ESVFP2/(R)EMVFP2 for
 334 open source (Relativistic) ElectroStatic/ElectroMagnetic Vlasov-Maxwell and Vlasov-Fokker-
 335 Planck-Maxwell in 2D 14) implement the Perfectly Matched Layer (PML) technique (Berenger,
 336 1994) to absorb the electromagnetic fields at the spatial simulation box boundaries 15) deploy
 337 the code to GPU architectures.

338 Figures

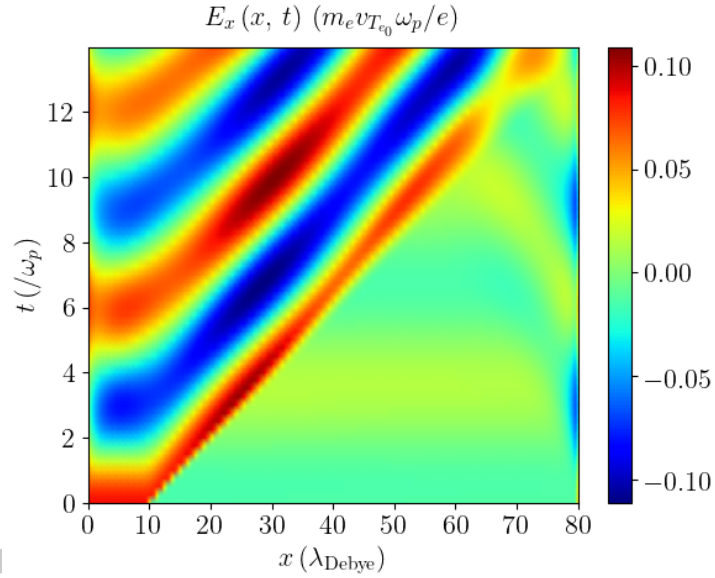


Figure 1: Electrostatic wakefield test case : Electrostatic wakefield $E_x(x, t)$ emitted by a Gaussian electron propagating in a collisionless plasma at Maxwell-Boltzmann equilibrium Equation 27 and initialized according to Equation 28 with $A = 0.1$ and $\underline{v}_d = 5$.

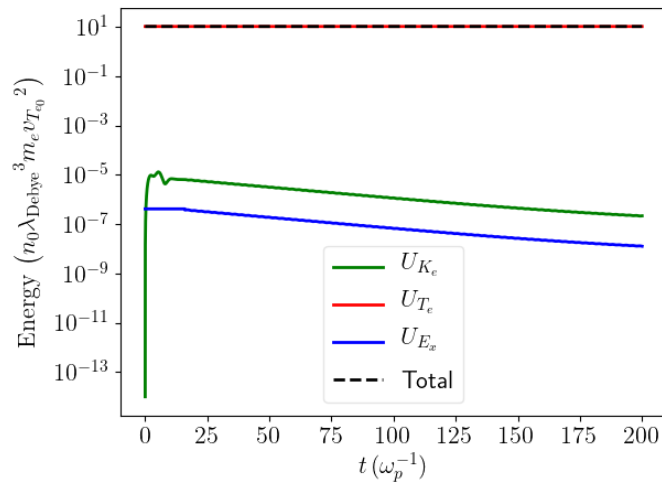


Figure 2: Linear Landau damping test case : Total electrostatic field energy and plasma electrons kinetic energy time evolution of the linearly Landau damped electron plasma wave propagating in the collisionless plasma at Maxwell-Boltzmann equilibrium Equation 27 and initialized according to Equation 29 with $A = 10^{-3}$, $\underline{k} = 0.29919930034$ and $\underline{\omega}_0 = 1.18$.

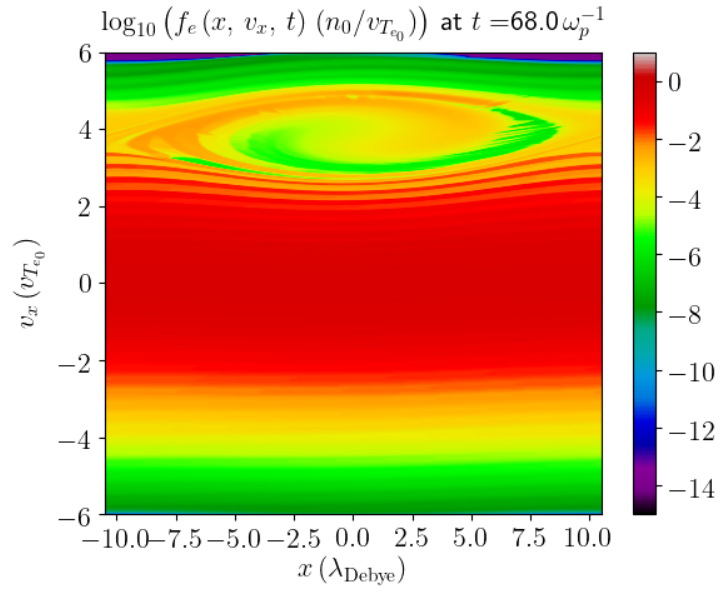


Figure 3: Non Linear Landau damping test case : Plasma electrons phase-space $f_e(x, v_x, t = 68)$ in the non-linear Landau damping of the electron plasma wave propagating in the collisionless plasma at Maxwell-Boltzmann equilibrium Equation 27 and initialized according to Equation 29 with $A = 10^{-1}$, $\underline{k} = 0.29919930034$ and $\underline{\omega}_0 = 1.18$.

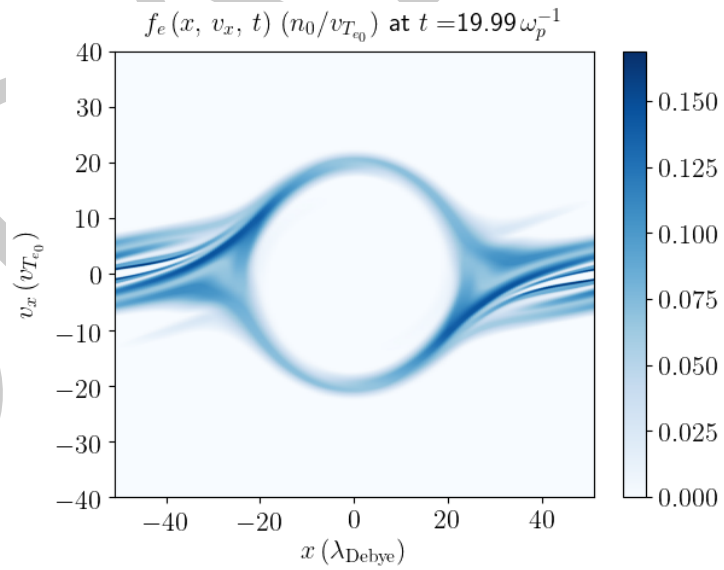


Figure 4: Two stream instability test case : Plasma electrons phase-space $f_e(x, v_x, t = 19.99)$ in the two-stream instability of two counter-propagating electron beams initialized according to Equation 34 with $A = 10^{-1}$, $\underline{k} = 0.06159985595$ ($\underline{x}_{\min} = -\underline{x}_{\max} = 51$) and $\underline{v}_d = 10$.

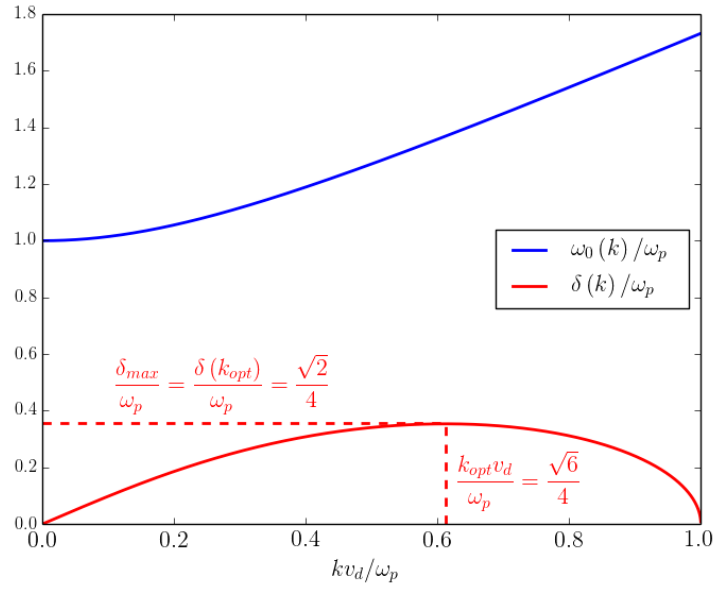


Figure 5: Two stream instability test case : Stationary electron plasma waves angular frequency Equation 52 seeded by the perturbation Equation 35 and the two-stream instability growth rate Equation 54 as a function of the spatial angular frequency mode k .

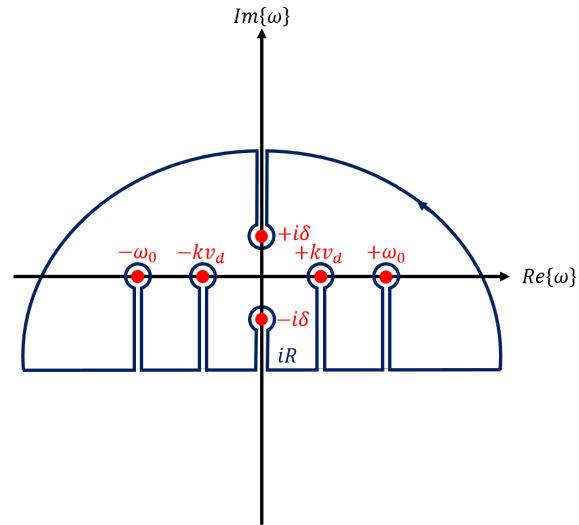


Figure 6: Two stream instability test case : Integration contour used to evaluate the the Cauchy principal value of the integral Equation 56.

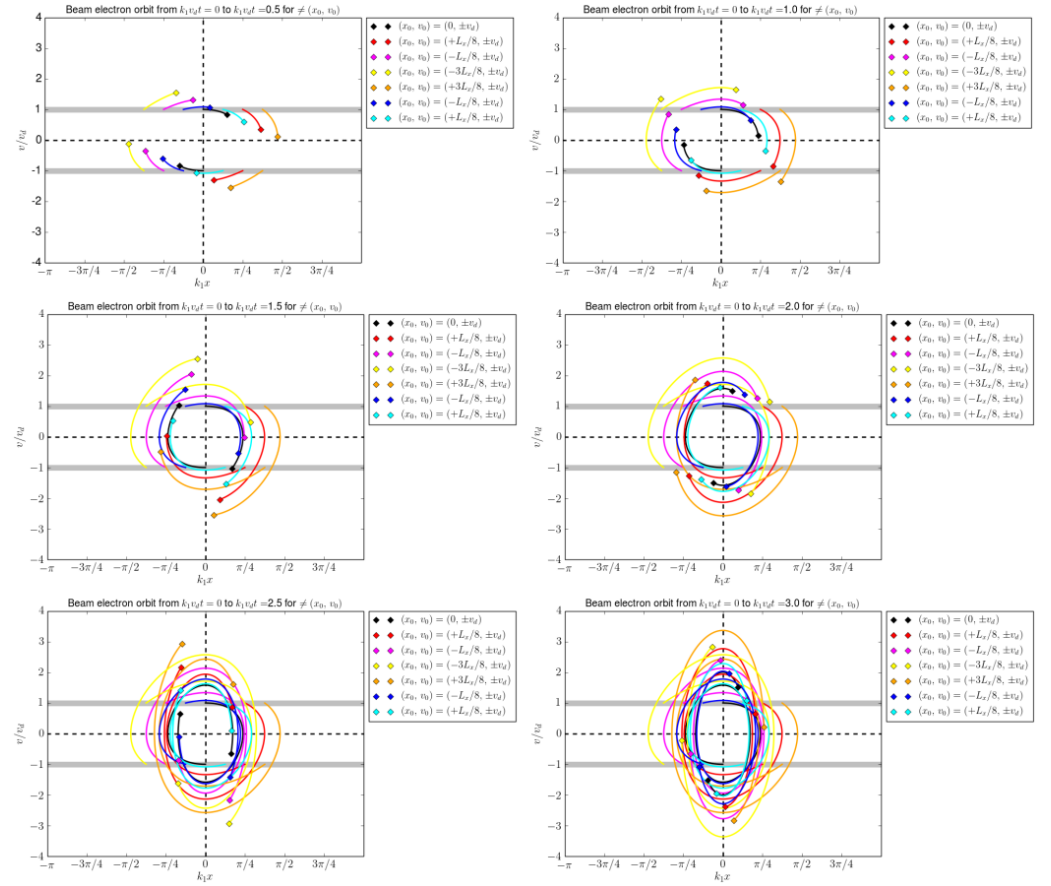


Figure 7: Two stream instability test case : Some beam electron orbits according to analytical estimates Equation 78 and Equation 79.

References

- Beam, R. M., & Warming, R. F. (1976). An implicit finite-difference algorithm for hyperbolic systems in conservation-law form. *Journal of Computational Physics*, 22(1), 87–110. [https://doi.org/10.1016/0021-9991\(76\)90110-8](https://doi.org/10.1016/0021-9991(76)90110-8)
- Belaiev, S. T., & Budker, G. I. (1956). *Dokl. Akad. Nauk SSSR*, 107.
- Berenger, J.-P. (1994). A perfectly matched layer for the absorption of electromagnetic waves. *Journal of Computational Physics*, 114(2), 185–200. <https://doi.org/10.1006/jcph.1994.1159>
- Bernstein, I. B., Greene, J. M., & Kruskal, M. D. (1957). Exact nonlinear plasma oscillations. *Phys. Rev.*, 108, 546–550. <https://doi.org/10.1103/PhysRev.108.546>
- Bhatnagar, P. L., Gross, E. P., & Krook, M. (1954). A model for collision processes in gases. I. Small amplitude processes in charged and neutral one-component systems. *Phys. Rev.*, 94, 511–525. <https://doi.org/10.1103/PhysRev.94.511>
- Braams, B. J., & Karney, C. F. F. (1987). Differential form of the collision integral for a relativistic plasma. *Phys. Rev. Lett.*, 59, 1817–1820. <https://doi.org/10.1103/PhysRevLett.59.1817>
- Courant, R., Friedrichs, K., & Lewy, H. (1928). Über die partiellen differenzengleichungen der mathematischen. *Physik. Math. Ann.*, 100, 32–74. <https://doi.org/10.1007/BF01532760>

- 357 [10.1007/BF01448839](https://doi.org/10.1007/BF01448839)
- 358 Courant, R., Isaacson, E., & Rees, M. (1952). On the solution of nonlinear hyperbolic differ-
359 ential equations by finite differences. *Communications on Pure and Applied Mathematics*,
360 5(3), 243–255. <https://doi.org/https://doi.org/10.1002/cpa.3160050303>
- 361 Crouseilles, N., & Filbet, F. (2004). Numerical approximation of collisional plasmas by high or-
362 der methods. *Journal of Computational Physics*, 201(2), 546–572. <https://doi.org/https://doi.org/10.1016/j.jcp.2004.06.007>
- 363 <https://doi.org/https://doi.org/10.1016/j.jcp.2004.06.007>
- 364 Dawson, J. (1962). One-dimensional plasma model. *The Physics of Fluids*, 5(4), 445–459.
365 <https://doi.org/https://doi.org/10.1063/1.1706638>
- 366 de Buyl, P. (2014). The vmf90 program for the numerical resolution of the vlasov equa-
367 tion for mean-field systems. *Computer Physics Communications*, 185(6), 1822–1827.
368 <https://doi.org/https://doi.org/10.1016/j.cpc.2014.03.004>
- 369 Debye, P., & Hückel, E. (1923). Zur theorie der elektrolyte. I. Gefrierpunktserniedrigung und
370 verwandte erscheinungen. *Z. Phys.*, 24, 305–324.
- 371 Decyk, V. K. (1987). Simulation of microscopic processes in plasma. *Proc. 1987 International*
372 *Conference on Plasma Physics, Kiev, USSR, April 1987, Ed. A G Sitenko [World Scientific,*
373 *Singapore, 1987] Vol. II, p. 1075.*
- 374 Derouillat, J., Beck, A., Pérez, F., Vinci, T., Chiaramello, M., Grassi, A., Flé, M., Bouchard,
375 G., Plotnikov, I., Aunai, N., Dargent, J., Riconda, C., & Grech, M. (2018). Smilei :
376 A collaborative, open-source, multi-purpose particle-in-cell code for plasma simulation.
377 *Computer Physics Communications*, 222, 351–373. <https://doi.org/https://doi.org/10.1016/j.cpc.2017.09.024>
- 378 <https://doi.org/https://doi.org/10.1016/j.cpc.2017.09.024>
- 379 Duclous, R., Dubroca, B., Filbet, F., & Tikhonchuk, V. (2009). High order resolution of the
380 maxwell–fokker–planck–landau model intended for ICF applications. *Journal of Computa-*
381 *tional Physics*, 228(14), 5072–5100. <https://doi.org/https://doi.org/10.1016/j.jcp.2009.04.005>
- 382 <https://doi.org/https://doi.org/10.1016/j.jcp.2009.04.005>
- 383 Fried, B. D., & Conte, S. D. (1961). Elsevier.
- 384 Fromm, J. E. (1968). A method for reducing dispersion in convective difference schemes.
385 *Journal of Computational Physics*, 3(2), 176–189. [https://doi.org/https://doi.org/10.1016/0021-9991\(68\)90015-6](https://doi.org/https://doi.org/10.1016/0021-9991(68)90015-6)
- 386 [https://doi.org/https://doi.org/10.1016/0021-9991\(68\)90015-6](https://doi.org/https://doi.org/10.1016/0021-9991(68)90015-6)
- 387 Godunov, S. K. (1959). Eine differenzenmethode für die näherungsberechnung unstetiger
388 lösungen der hydrodynamischen gleichungen. *Mat. Sb., Nov. Ser.*, 47, 271–306.
- 389 Gould, R. W., O’Neil, T. M., & Malmberg, J. H. (1967). Plasma wave echo. *Phys. Rev.*
390 *Lett.*, 19, 219–222. <https://doi.org/https://doi.org/10.1103/PhysRevLett.19.219>
- 391 Joglekar, A. S., & Levy, M. C. (2020). VlaPy: A python package for eulerian vlasov-poisson-
392 fokker-planck simulations. *Journal of Open Source Software*, 5(53), 2182. <https://doi.org/https://doi.org/10.21105/joss.02182>
- 393 <https://doi.org/https://doi.org/10.21105/joss.02182>
- 394 Landau, L. D. (1937). *JETP*, 7, 203.
- 395 Landau, L. D., & Lifshitz, E. M. (1981). *Physical kinetics* (Vol. 10). Pergamon Press.
- 396 Lax, P., & Wendroff, B. (1960). Systems of conservation laws. *Communications on Pure*
397 *and Applied Mathematics*, 13(2), 217–237. <https://doi.org/https://doi.org/10.1002/cpa.3160130205>
- 398 <https://doi.org/https://doi.org/10.1002/cpa.3160130205>
- 399 Liu, X.-D., Osher, S., & Chan, T. (1994). Weighted essentially non-oscillatory schemes.
400 *Journal of Computational Physics*, 115(1), 200–212. <https://doi.org/https://doi.org/10.1006/jcph.1994.1187>
- 401 <https://doi.org/https://doi.org/10.1006/jcph.1994.1187>
- 402 Roe, P. L. (1986). Characteristic-based schemes for the euler equations. *Annual Review of*
403 *Fluid Mechanics*, 18(1), 337–365. <https://doi.org/https://doi.org/10.1146/annurev.fl.18.010186.002005>

- 404 Rosenbluth, M. N., MacDonald, W. M., & Judd, D. L. (1957). Fokker-planck equation for
405 an inverse-square force. *Phys. Rev.*, 107, 1–6. <https://doi.org/10.1103/PhysRev.107.1>
- 406 Sagdeev, R. Z., & Galeev, A. A. (1969). *Nonlinear Plasma Theory*. W. A. Benjamin, Inc.,
407 New York.
- 408 Touati, M., Feugeas, J.-L., Nicolai, P., Santos, J. J., Gremillet, L., & Tikhonchuk, V. T.
409 (2014). A reduced model for relativistic electron beam transport in solids and dense
410 plasmas. *New Journal of Physics*, 16(7), 073014. [https://doi.org/10.1088/1367-2630/](https://doi.org/10.1088/1367-2630/16/7/073014)
411 [16/7/073014](https://doi.org/10.1088/1367-2630/16/7/073014)
- 412 Tzoufras, M., Bell, A. R., Norreys, P. A., & Tsung, F. S. (2011). A vlasov–fokker–planck code
413 for high energy density physics. *Journal of Computational Physics*, 230(17), 6475–6494.
414 [https://doi.org/https://doi.org/10.1016/j.jcp.2011.04.034](https://doi.org/10.1016/j.jcp.2011.04.034)
- 415 van Leer, B. (1979). Towards the ultimate conservative difference scheme. V. A second-
416 order sequel to godunov's method. *Journal of Computational Physics*, 32(1), 101–136.
417 [https://doi.org/https://doi.org/10.1016/0021-9991\(79\)90145-1](https://doi.org/10.1016/0021-9991(79)90145-1)
- 418 Van Leer, B. (1977). Towards the ultimate conservative difference scheme III. Upstream-
419 centered finite-difference schemes for ideal compressible flow. *Journal of Computational*
420 *Physics*, 23(3), 263–275. [https://doi.org/https://doi.org/10.1016/0021-9991\(77\)](https://doi.org/10.1016/0021-9991(77)90094-8)
421 [90094-8](https://doi.org/10.1016/0021-9991(77)90094-8)
- 422 Vlasov, A. A. ;. (1938). *JETP*, 8(3), 291.
- 423 Yee, K. (1966). *IEEE Transactions on Antennas and Propagation*, 14(3), 302–307. <https://doi.org/10.1109/TAP.1966.1138693>
424 <https://doi.org/10.1109/TAP.1966.1138693>